Early postnatal inhibitory circuit development in the mouse medial prefrontal and primary somatosensory cortex

Katerina Kalemaki[1,2], Xiaxia Xu[3], Ileana L. Hanganu-Opatz[3], Kyriaki Sidiropoulou[2,4*] and Domna Karagogeos[1, 2*]

[1]Department of Basic Science, Faculty of Medicine, University of Crete, Heraklion, Greece
[2]Institute of Molecular Biology and Biotechnology (IMBB), FORTH, Heraklion, Greece
[3]Developmental Neurophysiology, Institute of Neuroanatomy, University Medical Center Hamburg-Eppendorf, Hamburg, Germany
[4]Department of Biology, University of Crete, Heraklion, Greece
[*] co-corresponding author and equal senior contribution

Abstract

The prefrontal cortex (PFC) is characterized by delayed maturation that extends until adulthood. Although the adolescent PFC has been well investigated, the cellular mechanisms controlling the early development of prefrontal circuits are still largely unknown. Our study delineates the developmental cellular processes that are on-going in the mouse medial PFC (mPFC) during the second and third postnatal weeks and compares them to those in the barrel cortex (BC). We show that basal synaptic transmission decreases from the second to the third postnatal week in both brain areas due to increased spontaneous inhibitory currents and reduced excitatory ones. Furthermore, increasing $GABA_A$ receptor ($GABA_AR$) activity leads to increased basal synaptic response of neonatal mPFC, but not BC. Additionally, the K-Cl co-transporter 2 (KCC2) expression is decreased in the neonatal mPFC compared to the pre-juvenile one as well as to the neonatal and pre-juvenile BC, suggesting that $GABA_AR$ function in the neonatal mPFC is non-inhibitory. Moreover, the intrinsic properties of both interneurons and pyramidal cells change with age and relate to augmented network activity across development.

Keywords: development, prefrontal cortex, barrel cortex, $GABA_AR$, interneurons, KCC2.

Abbreviations

BC: Barrel Cortex

mPFC: medial Prefrontal Cortex

P10: Postnatal day 10

PNs: Pyramidal neurons

INs: Interneurons

Introduction

During early postnatal development, major events that contribute to cortical circuit maturation include spatial and temporal patterns of electrical activity, intrinsically determined cell death of early postnatal cortical interneurons and the depolarizing action of the neurotransmitter GABA (γ-aminobutyric acid)[1-9]. The developmental switch of GABA action from depolarizing to hyperpolarizing results from changes in chloride co-transporter expression: Na^+-K^+-Cl^- cotransporter 1 (NKCC1), the Cl^- importer, is highly expressed early in development, while the expression of the co-transporter KCC2, the Cl^- exporter, increases after the first postnatal week[10-13]. In addition, both intrinsic properties of neurons and synaptic transmission undergo dramatic changes during early postnatal development in a brain-area specific manner[14-18].

Most studies on these developmental changes of the GABAergic system in the cortex have focused on the primary somatosensory cortex, visual cortex and hippocampus[19-21]. The barrel cortex (BC) is part of the primary somatosensory cortex and is organised vertically in columns of cells associated with sensory perception[22] and horizontally in six layers of distinct cell types. In contrast, cortical association areas such as the prefrontal cortex (PFC) regulate cognitive functions and do not directly control sensory information[23]. Anatomically, the mouse medial PFC (mPFC) is defined as the agranular part of frontal lobe, lacking the prominent granular layer IV and is divided into distinct subregions, namely infralimbic, prelimbic and cingulate cortex [24,25]. The timeline of mPFC development is delayed compared to other sensory cortices, such as BC[26-28]. From infancy to adulthood, the developing mPFC undergoes considerable transcriptional, structural, neuronal changes[28-32].

While adolescent development of prefrontal circuitry and the underlying cellular mechanisms have been addressed by a large number of studies, only few investigations tackled the wiring processes at earlier stages[5,33,34]. However, specific knowledge is missing for the physiological and cellular changes that are on-going in the mPFC between the second

(neonatal) and third (pre-juvenile) postnatal week. Here, we aim to fill this gap by investigating the synaptic and intrinsic properties of neonatal and pre-juvenile mPFC neurons and comparing them to those in the BC, with a primary focus on the GABAergic system.

Results

Mice belonging to two age groups were investigated: (i) neonatal mice included pups of postnatal days (P) 9-11 and are defined as P10 while (ii) pre-juvenile mice defined as P20 animals including pups of P19-P21. Due to the high density of intra-cortical synapses in the superficial cortical layers[35,36], we focused on the superficial layers of the subdivision of the mPFC and on the superficial layers of the BC. From each mouse brain, both the mPFC and the BC were studied. All analyses that had four groups (mPFC P10 and P20, BC P10 and P20) were conducted using two-way ANOVA, with the two factors being the brain area (mPFC and BC) and age (P10 and P20).

Synaptic transmission decreased in mPFC and BC across development

First, we investigated the synaptic properties of mPFC and BC in neonatal compared to juvenile mice. We measured basal synaptic transmission using extracellular field recordings in brain slices. The evoked field excitatory postsynaptic potentials (fEPSPs) in layer II/III of both areas were recorded in response to current pulses of increasing intensity through the stimulating electrodes in layer II/III (**Figure 1a,c**). The fEPSPs were significantly decreased in both mPFC and BC at P20 compared to P10 (**Figure 1b,d**).

The decreased fEPSP responses at P20, compared to P10 (**Figure 1b,d**), could result from either increased inhibitory postsynaptic currents or decreased excitatory postsynaptic currents. To examine this, we performed patch-clamp recordings from layer II/III pyramidal neurons in mPFC and BC from P10 and P20 mice. We recorded spontaneous inhibitory postsynaptic currents (sIPSCs) at +10mV) and spontaneous excitatory postsynaptic currents (sEPSCs) at -60mV) and we measured the frequency, amplitude and decay time constant.

In mPFC, the frequency of sIPSCs was significantly augmented at P20 compared to P10 (**Figure 2a,b**), while the sIPSC amplitude and decay-time constant did not significantly change over the investigated time window (**Figure 2a,c,d**). In BC, sIPSC frequency and amplitude were significantly increased, at P20 compared to P10 (**Figure 2a,b,c**), while the decay-time constant was not altered (**Figure 2a,d**). When comparing the two brain areas, we noticed a significantly

lower sIPSC frequency in the mPFC compared to BC at both ages (**Figure 2a**). The decay time constant were similar (**Figure 2a,d**), while the sIPSC amplitude was significantly smaller at P20 in the mPFC compared to BC (**Figure 2a,b**).

The sEPSC frequency was significantly decreased at P20 compared to P10, in both areas (**Figure 2e,f**), while the amplitude and decay time constant were unaltered (**Figure 2e,g,h**). Upon comparing the two brain areas, the sEPSC frequency and amplitude were found significantly decreased in mPFC, compared to BC, at P10 (**Figure 2e,f**). At P20, the sEPSC frequency was similar between the two cortical areas, while the amplitude remained significantly smaller in mPFC compared to BC in both ages (**Figure 2e,g**). The decay time constant was not different between areas at both ages (**Figure 2e, h**).

The combination of reduced sEPSC and increased sIPSC frequency can underlie the fEPSP reduction from P10 to P20 in mPFC and BC (**Figure 1b,d**).

Figure 1

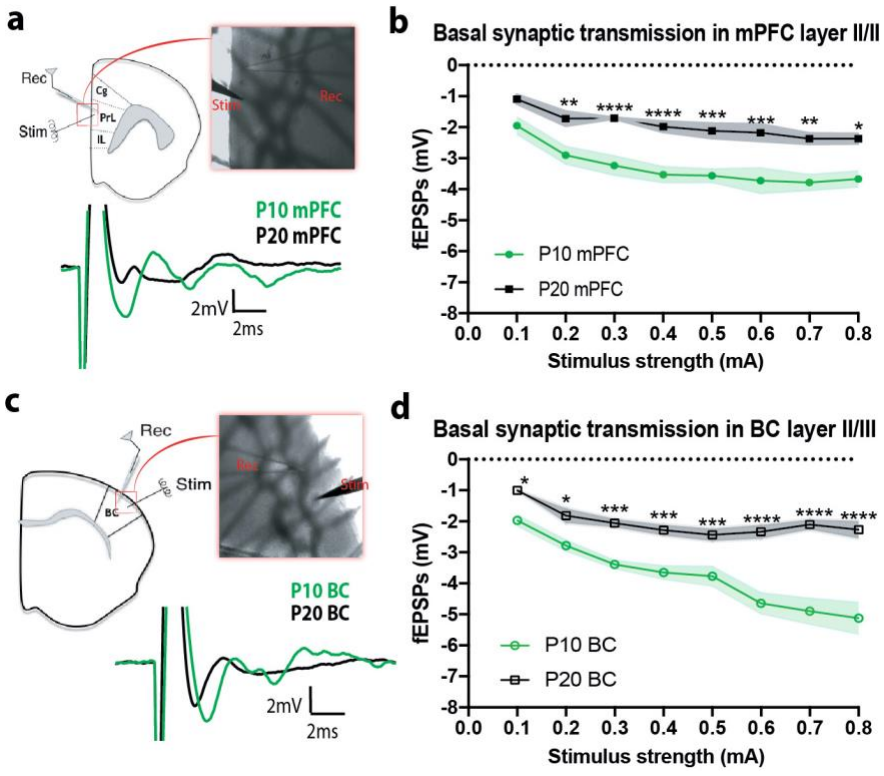

Figure 1. Basal Synaptic transmission is decreased in mPFC and BC across development

(**a, c**) (Top) Schematic representative photos showing the position of the electrodes in mPFC and BC brain slices (Rec: recording electrode, Stim: stimulating electrode). (Bottom) Representative traces showing the evoked field excitatory postsynaptic potentials (fEPSPs).

(**b,d**) Graphs showing the fEPSPs recorded in response to current pulses of increasing stimulus strength in layer II/III of mPFC (**b**) and BC (**d**). Two-way repeated measures ANOVA analyses of evoked fEPSPs revealed a significant effect of stimulus strength ($F_{(7, 82)}$ = 19.17, p<0.0001) and ages ($F_{(1, 82)}$ = 212.3, p<0.0001). Post-hoc analysis showed the fEPSPs significantly decreased at P20 compared to P10 in layer II/III of mPFC (Sidak's test, *p= 0.0106, **p=0.0012, ***p=0.0003 and ****p<0.0001) and BC (Sidak's test, *p=0.0279, ***p=0.0006 and ****p <0.0001), (n=6-7 brain slices from 3-4 WT male mice).

Figure 2

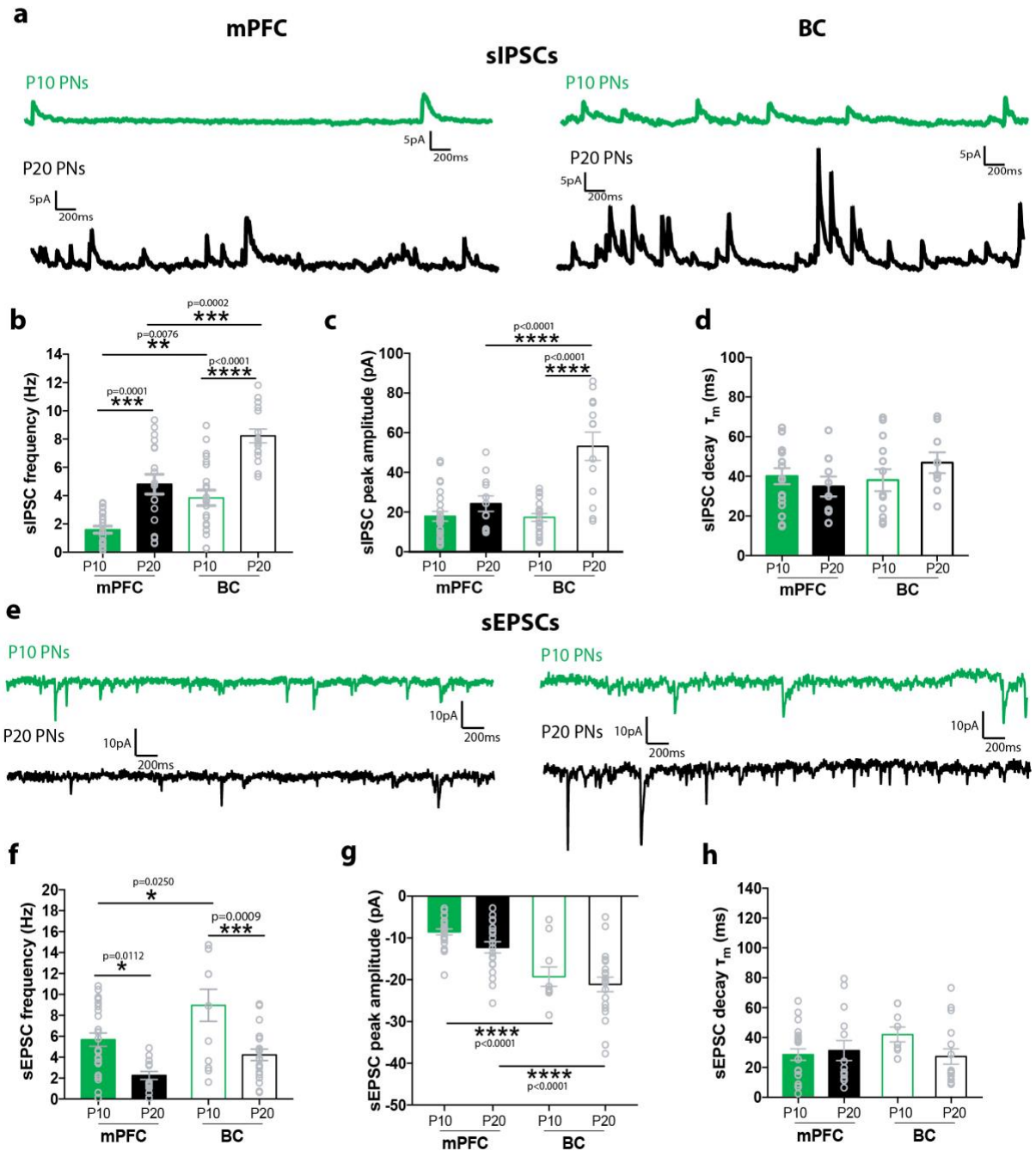

Figure 2. Properties of sIPSCs and sEPSCs at P10 and P20 of layer II/III mPFC and BC pyramidal neurons

(a) Representative traces of spontaneous inhibitory postsynaptic currents (sIPSCs) from layer II/III mPFC (left) and BC (right) pyramidal neurons at P10 (green) and P20 (black).

(b) Bar graph showing the sIPSC frequency (Hz) at P10 and P20 mPFC and BC pyramidal neurons. Two-way ANOVA analyses showed a significant effect of age ($F_{(1,74)}$=54.74, p<0.0001) and brain area ($F_{(1,74)}$=30.36, p<0.0001). Post-hoc analysis showed that sIPSC frequency was significantly increased at P20 compared to P10 in mPFC (Tukey's test, p=0.0001) as well as in BC (Tukey's test, p<0.0001). Furthermore, sIPSC frequency was significantly decreased in mPFC compared to BC at P10 (Tukey's test, p=0.0076) as well as at P20 (Tukey's test, p=0.0002), (n=9-13 cells from 5-9 mice/age group).

(c) Bar graph showing the sIPSC peak amplitude at P10 and P20 of mPFC and BC pyramidal neurons. Two-way ANOVA analyses showed a significant effect of age ($F_{(1,65)}$=30.78, p<0.0001) and brain area (($F_{(1,65)}$=13.85 p<0.0001). Post-hoc analysis showed that the sIPSC amplitude (pA) was significantly increased at P20 compared to P10 in BC (Tukey's test, p<0.0001) but not in mPFC (Tukey's test, p=0.63). The sIPSC amplitude was significantly decreased at P20 in mPFC compared to BC (Tukey's test, p<0.0001) but not at P10 between areas (Tukey's test, p=0.9993), (n=9-13 cells from 5-9 mice/age group).

(d) Bar graph showing the sIPSC decay time constant (τm) at P10 to P20 of mPFC and BC pyramidal neurons. Two-way ANOVA analyses did not show any significant effect of age ($F_{(1,45)}$= 0.11, p=0.73) or brain area ($F_{(1, 45)}$ = 0.96, p=0.33) was found (n=9-13 cells from 5-9 mice/age group).

(e) Representative traces of spontaneous excitatory postsynaptic currents (sEPSCs) from layer II/III mPFC (left) and BC (right) pyramidal neurons at P10 (green) and P20 (black).

(f) Bar graph showing the sEPSC frequency at P10 to P20 of mPFC and BC pyramidal neurons. Two-way ANOVA analyses showed a significant effect of age ($F_{(1,68)}$=26.8, p<0.0001) and brain area ($F_{(1,68)}$=10,82 p=0.0016). Post-hoc analysis showed that the sEPSCs frequency significantly decreased at P20 compared to P10 in mPFC (Tukey's test, p= 0.0112) and BC (Tukey's test, p= 0.0009). Comparison of the two brain areas at P10, the sEPSCs frequency was significantly decreased in mPFC compared to BC (Tukey's test, p= 0.0250), (n=9-13 cells from 5-9 mice/age group).

(g) Bar graph showing the sEPSCs peak amplitude at P10 to P20 of mPFC and BC pyramidal neurons. Two-way ANOVA analyses showed a significant effect of brain area ($F_{(1,73)}$=42.7, p<0.0001) but not of age ($F_{(1,73)}$ = 3.435, p=0.067). The sEPSC amplitude was not significantly different at P10 and P20 in mPFC (Tukey's test, p= 0.1918) and BC (Tukey's test, p=0.8617). On the other hand, the sEPSC amplitude was significantly decreased in mPFC compared to BC at P10 and P20 (Tukey's test, p<0.0001) (n=9-13 cells from 5-9 mice/age group).

(h) Bar graph showing the sEPSCs decay time constant (τm) at P10 to P20 of mPFC and BC pyramidal neurons. Two-way ANOVA analyses showed no significant effect of age ($F_{(1,57)}$ = 0.22, p=0.27) or brain area ($F_{(1,57)}$ = 0.77, p=0.39) (n=9-13 cells from 5-9 mice/age group).

Passive and active membrane properties of MGE-derived interneurons are altered in the mPFC across development

159 Changes in interneuron properties could underlie the increased sIPSC frequency. To
160 investigate this, we performed current-clamp recordings from layer II/III mPFC and BC of
161 Lhx6^{+} interneurons. For this reason, Lhx6-cre;ROSA26fl-STOP-fl-YFP mice were used in which
162 Lhx6^{+} interneurons express YFP. Lhx6 is expressed by all post-mitotic and mature MGE-
163 derived interneurons[37], therefore, YFP is expressed in MGE-derived interneurons, which
164 include interneurons that express parvalbumin (PV^{+}) and somatostatin (SST^{+}).
165 Upon analysis of the passive properties, we found a significant decrease in the input
166 resistance, a significant increase in the membrane capacitance and a trend towards decrease
167 of the membrane time constant in the mPFC at P20 compared to P10, but no difference in
168 the resting membrane potential (RMP) (**Figure 3, Table 1**). Compared to BC, the input
169 resistance and membrane time constant were significantly higher in mPFC, at P10 (**Figure 3**,
170 **Table 1**).
171 With regard to the active properties, the rate of rise (dv/dt) was significantly
172 increased, while the duration of AP (half-width) was significantly reduced at P20 compared to
173 P10 in mPFC (**Figure 4b-c, Table 1**). On the other hand, the amplitude, the rheobase, the
174 threshold of the AP and the amplitude and time of AHP were not different between P10 to
175 P20, in the mPFC (**Figure 4a,d-g, Table 1**). Compared to BC at P10, we observed that the AP
176 amplitude was significantly increased (**Figure 4a, Table 1**), while AHP amplitude was
177 significantly decreased in the mPFC (**Figure 4f, Table 1**). The increased rate of rise and the
178 decreased AP duration are possibly linked with the up-regulation of voltage-dependent
179 sodium channels during development[38], and in combination with the reduced AHP amplitude
180 suggest that the PFC MGE-interneurons at P10 are still quite immature, when compared with
181 adult PV^{+}/SST^{+} interneurons in mPFC[39,40].
182 Overall, these data indicate that some intrinsic properties of interneurons in mPFC are
183 regulated by age (from P10 to P20) reaching values that closer resemble adult MGE-derived
184 interneurons [39,40]. Therefore, the increased sIPSC frequency of mPFC pyramidal neurons
185 observed at P20, compared to P10 could partly be explained by these altered properties of
186 presynaptic interneurons.
187

Figure 3

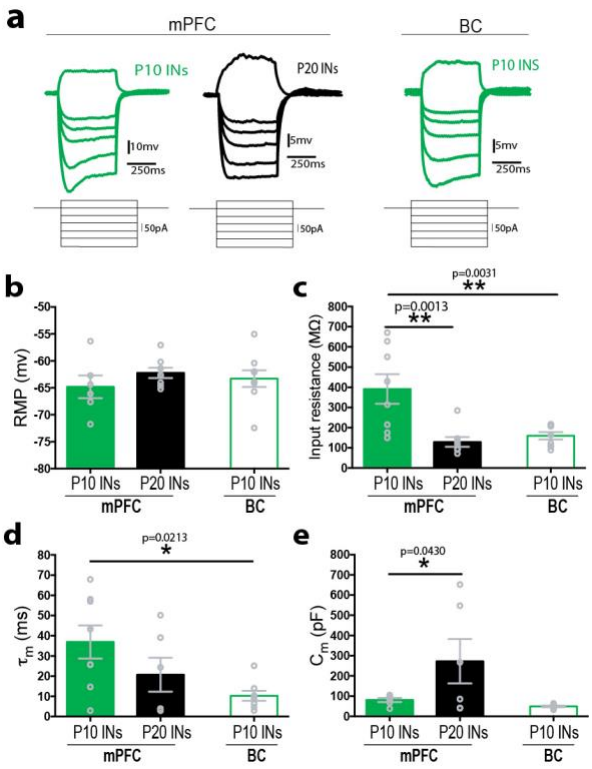

Figure 3. Passive membrane properties of Lhx6+ interneurons at P10 and P20 mPFC and P10 BC.

(a) Representative voltage responses (top traces) to 500ms positive and negative current pulses (bottom traces, +50, -50, -70, -100, -150, -200 pA) in mPFC at P10 and P20 and BC at P10 of Lhx6+ florescent interneurons from layer II/III.

(b) Bar graph showing the resting membrane potential (RMP) of interneurons at P10 and P20 in mPFC and at P10 in BC. One-way ANOVA analyses showed no significant effect among groups ($F_{(2, 20)} = 0.65$, p=0.5340), (n=6-9 cells from 5-6 mice/age group).

(c) Bar graph showing the input resistance of interneurons at P10 and P20 in mPFC and at P10 in BC. One-way ANOVA analyses showed significant effect among groups ($F_{(2, 22)}= 10.25$, p=0.0007). Post-hoc analysis showed that the input resistance significantly decreased at P20 compared to P10 in mPFC (Tukey's test, p=0.0013) and was significantly higher in mPFC compared with BC, at P10 (Tukey's test, p=0.0031), (n=8-9 cells from 5-6 mice/age group).

(d) Bar graph showing the membrane time constant (τm) of interneurons at P10 and P20 in mPFC and at P10 in BC. One-way ANOVA analyses showed significant effect among groups ($F (2, 19) = 4.41$, p=0.026). Post-hoc analysis showed that τm was not significantly altered at P20 compared to P20 in mPFC (Tukey's test, p=0.24) while it was significantly higher in mPFC compared to BC, at P10 (Tukey's test, p=0.021), (n=8-9 cells from 5-6 mice/age group).

(e) Bar graph showing the membrane capacitance (Cm) of interneurons at P10 and P20 in mPFC and at P10 in BC. One-way ANOVA analyses showed significant effect among groups ($F_{(2,16)}=4.0$, p=0.03). Post-hoc analysis

showed that Cm was significantly higher at P10 compared with P20 in mPFC (LSD test, p=0.04) and was not significantly different between mPFC and BC, at P10 (LSD test, p=0.7), (n=6-9 cells from 5-6 mice/age group).

Figure 4

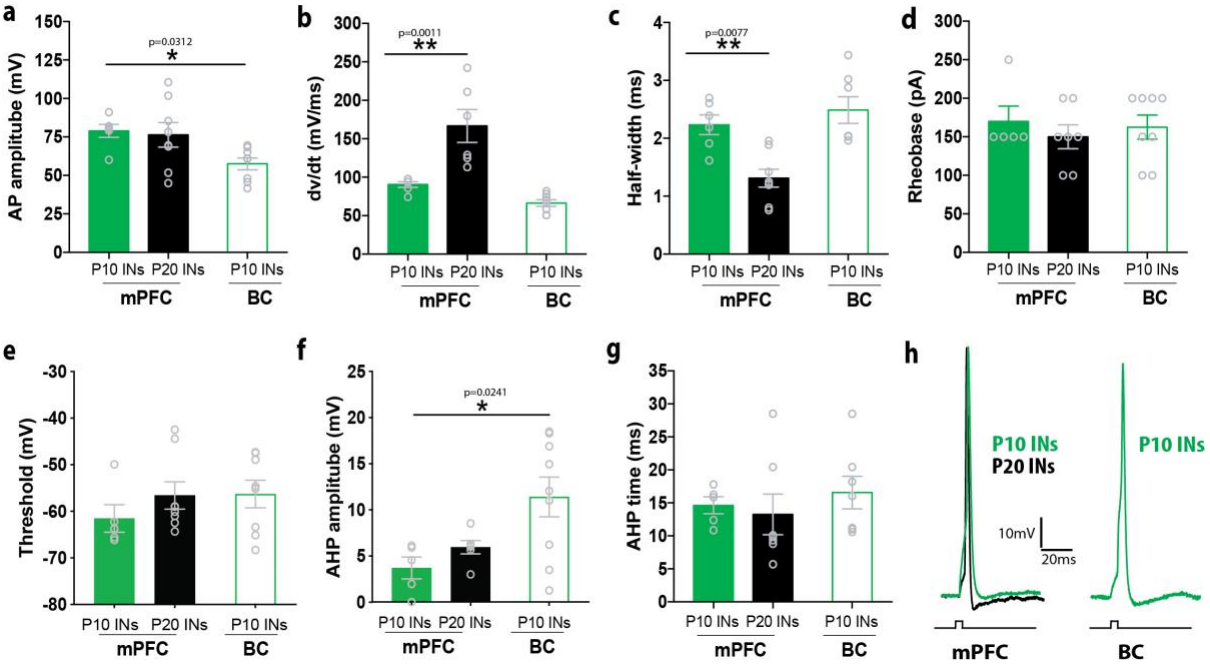

Figure 4. Poor development of active membrane properties of Lhx6⁺ interneurons in mPFC.

(a) Bar graph showing the action potential (AP) amplitude of interneurons at P10 and P20 in mPFC and at P10 in BC. One-way ANOVA analyses showed significant effect among groups ($F_{(2,19)}$=3.93, p=0.037). Post-hoc analysis showed that the AP amplitude was not significantly different at P20 compared to P10 in mPFC (Tukey's test, p= 0.76). Compared to BC, the AP amplitude was significantly higher in mPFC at P10 (Tukey's test, p= 0.03), (n=6-9 cells from 5-6 mice/age group).

(b) Bar graph showing the AP rate of rise (dv/dt) of interneurons at P10 and P20 in mPFC and at P10 in BC. One-way ANOVA analyses showed significant effect among groups ($F_{(2,17)}$=20.03, p<0.0001). Post-hoc analysis showed that the AP rate of rise significantly increased at P20 compared to P10 in mPFC (Tukey's test, p=0.0011) and was not significantly different in mPFC compared to BC, at P10 (Tukey's test, p=0.3), (n=6-9 cells from 5-6 mice/age group).

(c) Bar graph showing the AP duration (half-width) of interneurons at P10 and P20 in mPFC and at P10 in BC. One-way ANOVA analyses showed significant effect among groups ($F_{(2,18)}$= 11.69, p=0.0006). Post-hoc analysis showed that the AP duration significantly decreased at P20 compared to P10 in mPFC (Tukey's test, p= 0.0077) and was not significantly different between mPFC and BC, at P10 (Tukey's test, p=0.64), (n=6-9 cells from 5-6 mice/age group).

(d) Bar graph showing the AP rheobase of interneurons at P10 and P20 in mPFC and at P10 in BC. One-way ANOVA analyses showed no significant effect among groups ($F_{(2, 17)}$ = 0.33, p=0.7), (n=6-9 cells from 5-6 mice/age group, p=0.7).

(e) Bar graph showing the AP threshold of interneurons at P10 and P20 in mPFC and at P10 in BC. One-way ANOVA analyses showed no significant effect among groups ($F_{(2, 18)}$ = 0.7722, p=0.4767), (n=6-9 cells from 5-6 mice/age group).

(f) Bar graph showing the AHP (afterhypolarization) amplitude of interneurons at P10 and P20 in mPFC and at P10 in BC. One-way ANOVA analyses showed significant effect among groups ($F_{(2,17)}$ = 4.984, p=0.0198). Post-hoc analysis showed that the AHP amplitude was not significantly different at P20 compared to P10 in mPFC (Tukey's test, p=0.7167) and was significantly decreased in mPFC compered to BC, at P10 (Tukey's test, p= 0.0241), (n=6-9 cells from 5-6 mice/age group).

(g) Bar graph showing the AHP time of interneurons at P10 and P20 in mPFC and at P10 in BC. One-way ANOVA analyses showed no significant effect among groups ($F_{(2,16)}$=0.45, p=0.64), (n=6-9 cells from 5-6 mice/age group).

(h) Representative traces of APs of layer II/III Lhx6+ interneurons in mPFC (left) and BC (right) at P10 (green) and P20 (black).

The emergence of PV immunoreactivity is delayed in mPFC compared to BC

An additional explanation for the increased sIPSC frequency could come from alterations in interneuron cell densities. To test this, we quantified the number of interneurons per area in cryosections at P10 and P20 mPFC and BC coronal brain slices of Lhx6$^+$-expressing mice. In these, Lhx6$^+$ interneurons express YFP. The YFP$^+$ positive cells per area (i.e. Lhx6$^+$ cell density) in mPFC and BC was similar between ages, but was significantly reduced in the mPFC, compared to BC (**Figure 5a**).

The transcription factor Lhx6 is required for the specification and maintenance of main MGE-derived interneurons, PV and SST-positive interneuron subtypes, at postnatal ages[37]. The neuropeptide SST (both mRNA and protein) is progressively expressed from embryonic to postnatal levels[41,42]. We found that the SST mRNA levels were similar between areas and ages (**Figure 5b**). On the other hand, the emergence of PV immunoreactivity in the mouse cortex shows a delayed development, starting from early postnatal period to adult, with marked area-specific differences[43]. We found that PV was only immunoreactive in BC, and not in mPFC, at P10 (**Figure 5c and Supplementary Figure 1**). At P20, PV was immunoreactive in both mPFC and BC, but PV$^+$ cell density was significantly lower in the mPFC, compared to BC (**Figure 5c and Supplementary Figure 1**). Overall, the densities of Lhx6$^+$ and PV$^+$ cells are lower in the mPFC compared to BC, while SST$^+$ is not altered (**Supplementary Figure 2**).

We also counted the total cell density of mPFC and BC from neonatal and juvenile mice (**Supplementary Figure 3a**) using Nissl staining. In the mPFC the cell density significantly decreased at P20 compared to P10 (**Supplementary Figure 3b**). On the contrary, in BC, the

total cell density significantly increased at P20 compared to P10 (**Supplementary Figure 3b**) When the two brain areas were compared, no difference was found at P10, while the mPFC cell density was significantly decreased compared to BC at P20 (**Supplementary Figure 3b**).

We further examined whether the alterations in total cell density are derived from alterations in cell density of interneurons by measuring the Lhx6$^+$ neurons over the Nissl-positive cells. No differences were detected between areas and ages (**Supplementary Figure 3c**) suggesting that the changes in total cell density in mPFC and BC respectively are probably due to changes in other neuronal or glial populations.

Figure 5

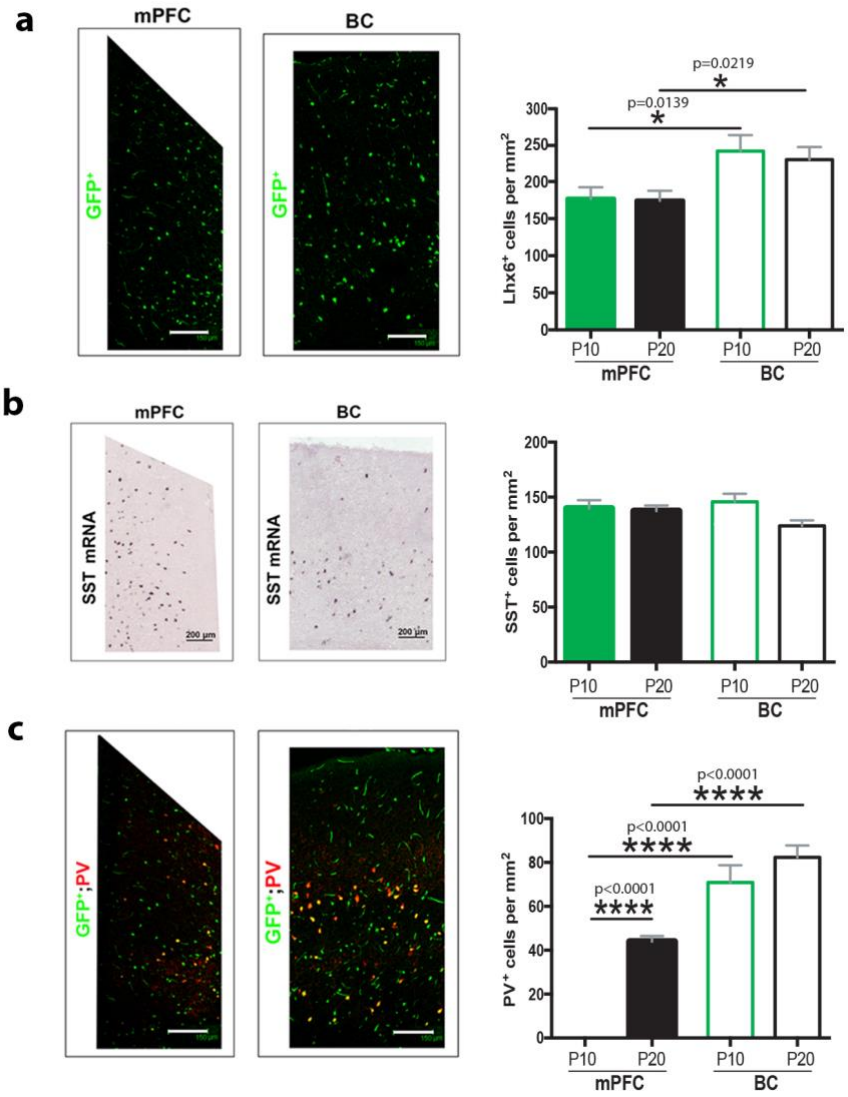

Figure 5. Significant differences in cellular density of Lhx6$^+$ interneurons in mPFC and BC at P10 and P20.

(a) A representative immunostaining with GFP for Lhx6$^+$ interneurons in Lhx6-cre;ROSA26fl-STOPfl-YFP mice in mPFC and BC at P20 is showing on the left. Scale bars: 150 µm. On the right, bar graph comparing Lhx6$^+$

interneurons cell density (per mm^2) at P10 and P20 in mPFC and BC. Two-way ANOVA analyses of the cell density revealed a significant effect of brain area ($F_{(1, 35)}$ = 12.47, p=0.0012), but not of age ($F_{(1,35)}$=0.1735, p=0.6795). Post-hoc analysis showed that the $Lhx6^+$ cell density was not significant different at P20 compared to P10 in mPFC and BC (LSD test, p=0.91 and p= 0.63, respectively). The $Lhx6^+$ cell density was significantly lower in mPFC compared to BC at P10 and P20, respectively (LSD test, p=0.01 and p= 0.02, respectively), (n=10-11 brain slices from 4-5 mice/age group).

(b) A representative in situ hybridization staining for somatostatin positive cells (SST^+) using wild type animals in mPFC and BC at P20 is showing on the left. Scale bar: 200µm. Bar graph comparing cell density based on SST^+ expression at P10 and P20 in mPFC and BC. Two-way ANOVA analyses of the cell density showed no significant effect of age ($F_{(1, 56)}$= 3.36, p=0.07) and brain area ($F_{(1,56)}$=0.29, p=0.59) was found, (n=12-17 brain slices from 4-5 mice/age group).

(c) A representative double immunostaining for GFP; PV (PV: parvalbumin) in mPFC and BC at P20 is showing on the left. Scale bars: 150 µm. On the right, bar graph comparing cell density based on PV^+ expression at P10 and P20 in mPFC and BC. Two-way ANOVA analyses of the cell density revealed a significant effect of age ($F_{(1, 18)}$ = 40.06, p<0.0001) and brain area ($F_{(1, 18)}$ = 156.2, p<0.0001). PV^+ cells were not found in mPFC but were identified in BC, at P10. Post-hoc analysis showed that the PV^+ cell density was not significantly different at P20 compared to P10 in BC (LSD test, p= 0.1089), but was significantly lower in mPFC compared to BC at P20 (LSD test, p<0.0001), (n=10-11 brain slices from 4-5 mice/age group).

GABA is non-inhibitory in the mPFC but not BC of neonatal mice

Our data so far have indicated several similarities in the development of mPFC and BC from the neonatal to pre-juvenile period, but also an indication for delayed maturation of several mPFC interneuron properties (intrinsic properties and PV immunoreactivity). Therefore, it is likely that another GABAergic developmental process is delayed, and specifically, that of the switch from depolarizing to hyperpolarizing function of $GABA_AR$. It is well known that $GABA_AR$ is depolarizing during the first postnatal week, but switches to hyperpolarizing at P7 in the hippocampus, cortex and amygdala[8,12,44-49]. Therefore, at P10, $GABA_AR$ function is inhibitory in the barrel cortex. We used diazepam (2µM) (a $GABA_AR$ agonist) to enhance $GABA_AR$ function and determine whether it is depolarizing by measuring the fEPSP response. At P10, diazepam did not significantly alter the fEPSP in BC, as expected if $GABA_AR$ function is inhibitory. However, diazepam increased the fEPSP amplitude in mPFC at P10 (**Figure 6a-b**). At P20, the fEPSP amplitude was not significantly altered following diazepam application in both mPFC and BC (**Figure 6c,d**). These results suggest that the $GABA_AR$ function is depolarizing in the mPFC at P10.

The switch in the $GABA_AR$ function from depolarizing to hyperpolarizing occurs due to the increased expression of the K^+-Cl^- co-transporter 2 (KCC2)[50]. Therefore, we measured KCC2 protein levels and demonstrated that they were significantly increased at P20 compared to P10 in the mPFC but not in the BC (**Figure 7a,b**). These results further support our hypothesis that the $GABA_AR$ function is depolarizing at P10 in the mPFC and could explain the observed increased fEPSPs and decreased sIPSCs.

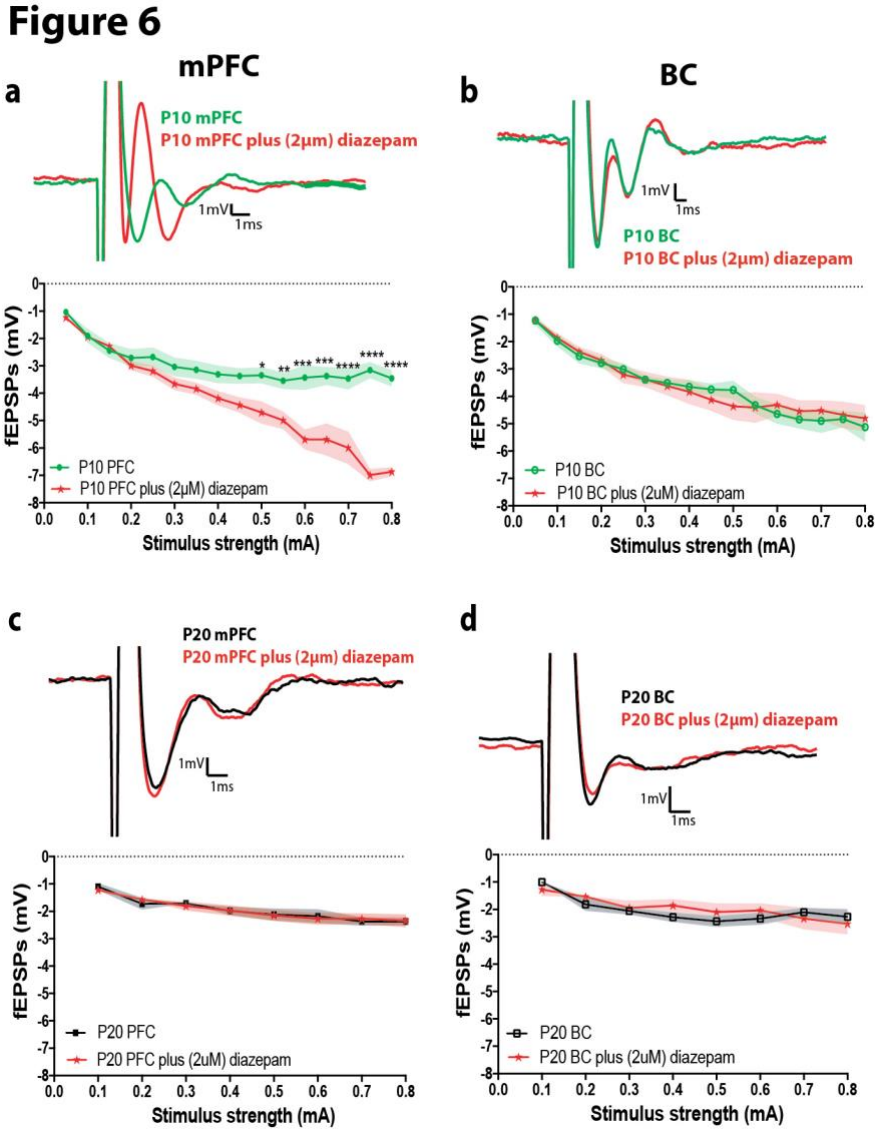

Figure 6. Increased $GABA_AR$ activity leads to enhanced fEPSPs in mPFC during the second postnatal week. fEPSPs were recorded were recorded in layer II/III in response to current pulses of increasing stimulus strength of layer II/III, during two experimental treatments, before and after application of 2µM diazepam ($GABA_AR$ agonist) at P10 and P20 of mPFC and BC in mice.

(a) Representative traces (left) and graph (right) showing the fEPSPs amplitude before (green) and after (red) diazepam bath application, in mPFC at P10. Two-way repeated measures ANOVA analyses of evoked fEPSPs revealed significant effect of stimulus strength ($F_{(15,135)} = 25.64$, $p<0.0001$) and experimental treatments ($F_{(1, 135)}$

= 136.1, p<0.0001). Post-hoc analysis showed that the fEPSP amplitude significantly increased in mPFC at P10 after diazepam bath application (Sidak's test, *p= 0.0175, **p=0.0082, ***p=0.0002 and ****p<0.0001 at 0.3, 0.4. 0.5, 0.6 and 0.7 mA respectively), (n=6-7 brain slices from 3-4 mice).

(b) Graph (right) and representative traces (left) showing that diazepam bath application does not have any effect on the fEPSP amplitude in BC at P10. Two-way repeated measures ANOVA analyses of evoked fEPSPs revealed a significant effect of stimulus strength (F (15, 140) = 24.05, p<0.0001) but not experimental conditions ($F_{(1, 135)}$ = 0.03, p=0.86), (n=6-7 brain slices from 3-4 mice).

(c) Graph (right) and representative traces (left) showing that diazepam bath application does not have any effect on the fEPSP amplitude in mPFC at P20. Two-way repeated measures ANOVA analyses of evoked fEPSPs revealed a significant effect of stimulus strength ($F_{(7, 96)}$ = 10.36, p<0.0001) but not experimental conditions ($F_{(1,96)}$=0.03, p=0.9382), (n=6-7 brain slices from 3-4 mice).

(d) Graph (right) and representative traces (left) showing that bath application of diazepam does not have any effect in the fEPSP amplitude in BC at P20. Two-way repeated measures ANOVA analyses of evoked fEPSPs revealed a significant effect of stimulus strength ($F_{(7, 96)}$ = 5.51, p<0.0001) but not experimental conditions ($F_{(1, 96)}$ = 0.50, p=0.47), (n=6-7 brain slices from 3-4 mice).

Figure 7

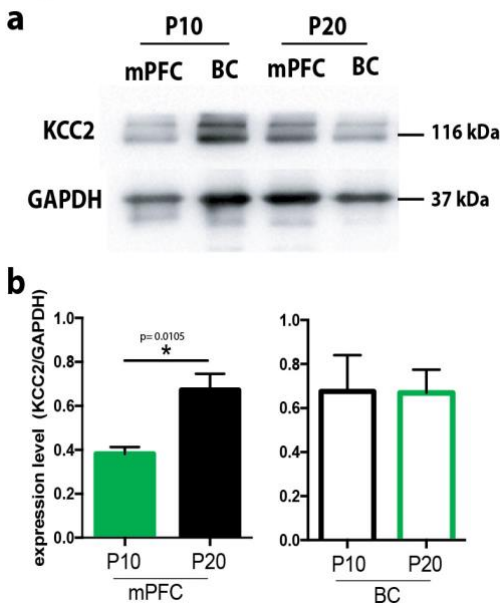

Figure 7. Decreased levels of K+-Cl- co-transporter 2 (KCC2) in mPFC during the second postnatal week.

(a) Representative blots showing changes of the K-Cl co-transporter (KCC2) levels, relative to GAPDH at P10 and P20 in mPFC and BC.

(b) Graph showing the normalized protein level (KCC2/GAPDH) in mPFC and BC at P10 and P20. The KCC2 protein levels was significantly increased at P20 compared to P10 in mPFC (two-tailed t-test, p= 0.01) but not in BC (two-tailed t-test, p= 0.97) (n=3-4 mice).

No significant changes in pyramidal neuron excitability

To determine whether the reduced sEPSC frequency can be explained by changes in pyramidal neuron excitability, we investigated their intrinsic properties. The passive and active properties of these neurons were measured using current-clamp recordings from layer II/III mPFC and BC pyramidal neurons. With regards to passive properties, no significant differences were observed in the RMP, the input resistance and the membrane time constant between brain regions and ages (**Supplementary Figure 4, Table 1**). Only the membrane capacitance was significantly increased at P20 compared to P10 (**Supplementary Figure 4d, Table 1**), in both brain areas. In addition, the number of spikes generated with increasing current stimulation was not significantly different between ages and regions (**Supplementary Figure 5**).

In terms of active properties, the AP amplitude and rate of rise were increased at P20 compared to P10 mPFC, while the AP half-width, rheobase and threshold were not significantly different (**Figure 8, Table 1**). The AP amplitude was also significantly increased at P20, compared to P10 in BC, while the other properties did not change (**Figure 8, Table 1**). Comparing the two regions at the two ages, we found no significant differences of AP properties of pyramidal neurons (**Figure 8, Table 1**). The developmental increase of AP amplitude and rate of rise in the mPFC could be due to the on-going maturation of sodium channels in pyramidal neurons. However, these changes could not account for the reduced sEPSCs in the neonatal, compared to pre-juvenile, mPFC and BC.

Figure 8

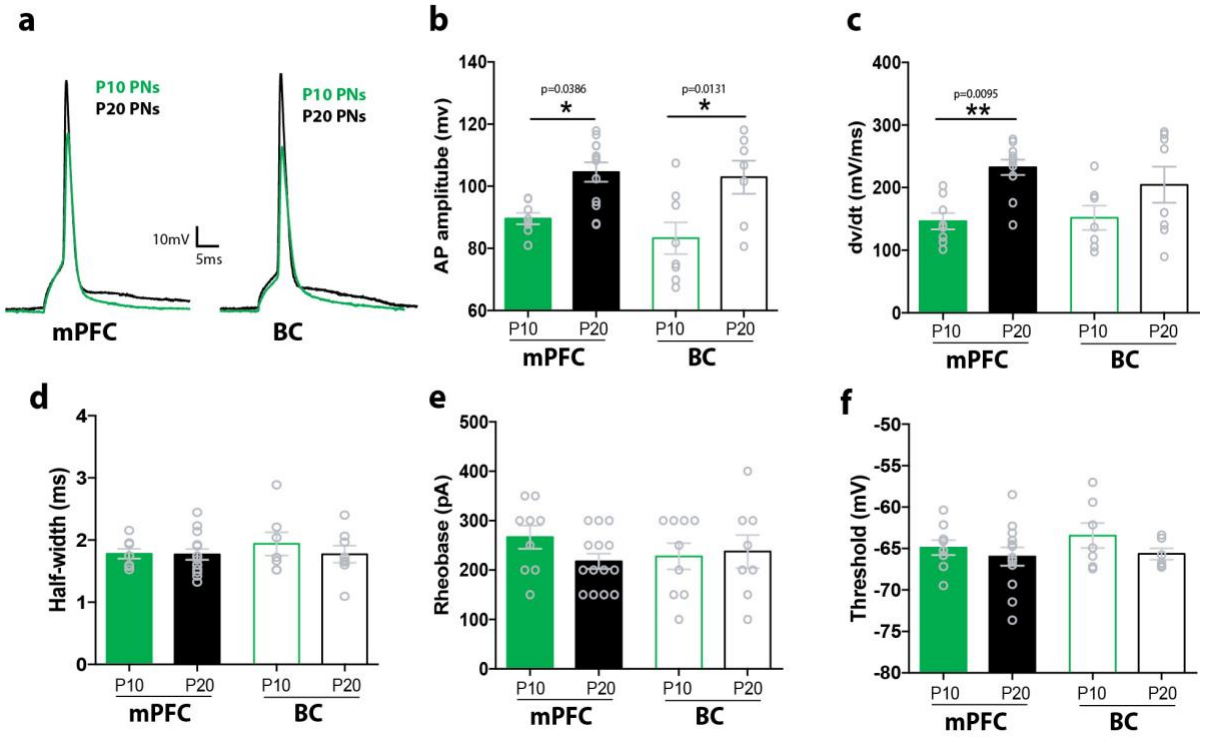

Figure 8. Active properties of mPFC and BC pyramidal neurons.

(a) Representative traces of action potentials (APs) of layer II/III pyramidal neurons in mPFC (left) and BC (right) at P10 (green) and P20 (black), respectively.

(b) Bar graph showing the AP amplitude of pyramidal neurons at P10 and P20 in mPFC and BC. Two-way ANOVA analyses showed a significant effect of age ($F_{(1, 31)}$ = 18.74, p=0.0001) but not on brain area ($F_{(1, 31)}$ = 0.99, p=0.32) was found. Post-hoc analysis showed that the AP amplitude significantly increased at P20 compared to P10 in mPFC and BC (Tukey's test, p=0.0386 and p= 0.0131, respectively) (n=9-14 cells from 6-10 mice/age group).

(c) Bar graph showing the AP rate of rise (dv/dt) of pyramidal neuron at P10 and P20 in mPFC and BC. Two-way ANOVA analyses showed a significant effect of age ($F_{(1,30)}$= 13.53, p=0.0009) but not on brain area ($F_{(1, 30)}$ = 0.36, p=0.55) was found. Post-hoc analysis showed that the AP rate of rise significantly increased at P20 compared to P10 in mPFC (Tukey's test, p= 0.0095), but not in BC (Tukey's test, p= 0.25) (n=8-14 cells from 6-10 mice/age group).

(d) Bar graph showing the AP duration (half-width) of pyramidal neuron at P10 and P20 in mPFC and BC. Two-way ANOVA analyses showed no significant effect of age (F(1, 33) = 0.52, p=0.47) or brain area ($F_{(1, 33)}$ = 0.43, p=0.51) was found (n=9-14 cells from 6-10 mice/age group).

(e) Bar graph showing the AP rheobase of pyramidal neuron at P10 and P20 in mPFC and BC. Two-way ANOVA analyses showed no significant effect of age ($F_{(1, 36)}$ = 0.66, p=0.41) or brain area ($F_{(1, 36)}$ = 0.16, p=0.69) was found (n=9-14 cells from 6-10 mice/age group).

(f) Bar graph showing the AP threshold of pyramidal neuron at P10 and P20 in mPFC and BC. Two-way ANOVA analyses showed no significant effect of age ($F_{(1,31)}$ = 1.90, p=0.17) or brain area ($F_{(1,31)}$=0.55, p=0.46) was found (n=9-14 cells from 6-10 mice/age group).

Increased firing activity *in vivo* in the mPFC between the second and third postnatal weeks

To investigate the physiological network activity *in vivo*, multisite recordings of the LFP and multi-unit activity (MUA) were performed in layers II/III of mPFC at P8-10 and P20-23. A significant increase of MUA was identified at P22 compared to P9 mice, indicating a developmental increased spiking activity in layers II/III of mPFC on the third compared to the second postnatal week. These results corroborate the increased AP amplitude and rate-of-rise of P20 mPFC pyramidal neurons (**Figure 9, Table 1**) and provide further evidence that the decreased synaptic activity of mPFC circuits cannot be attributed to increased spiking activity of mPFC neurons at P10.

Figure 9

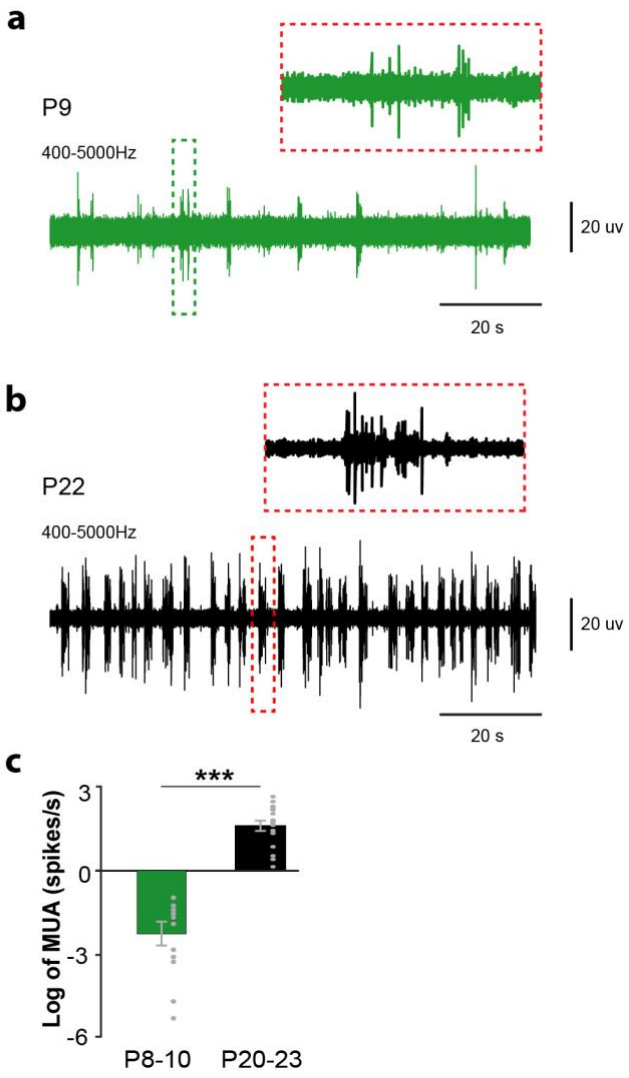

Figure 9. Spike activity in PFC of neonatal and pre-juvenile mice.

(a) Example of spike activity in PFC of a P9 mouse. The trace is extracellular LFP recordings after bandpass (500 -5000 Hz) filtering.

(b) the same display as (**a**), but in one P22 mouse.

(c) Bar diagram displaying the mean MUA of neurons in PFC of neonatal and pre-juvenile mice. During development, significant increase of MUA in PFC in pre-juvenile mice (n=14) compared with in neonatal mice (n=13) (1.71±0.16 vs. -2.29±0.45, $p<0.0001$, One way ANOVA, $F_{(1, 25)}=80.19$).

Discussion

Our study has identified significant developmental events in the mPFC and the BC between the second and third postnatal weeks. Specifically, we have shown that the basal synaptic transmission decreases from the second to the third postnatal week, a fact that can be explained by a concurrent decrease in the sEPSCs and an increase in the sIPSCs in both

mPFC and BC. Moreover, our data support a depolarizing action of $GABA_AR$ in the second postnatal week, in the mPFC only, as indicated by increased basal synaptic transmission following $GABA_AR$ activation and decreased protein levels of KCC2. In parallel, the intrinsic properties of both interneurons and pyramidal cells change with age and relate to augmented network activity across development.

Depolarizing GABA

GABA plays a crucial role in inhibiting adult neurons, acting primarily via the chloride-permeable $GABA_AR$ and resulting in hyperpolarization of the membrane potential[51]. However, GABA action leads to depolarization of immature neurons (i.e. during the first postnatal week in mice), due to an initially higher intracellular chloride concentration $[Cl^-]_{in}$[10-12]. The developmental switch of GABA action from depolarizing to hyperpolarizing results from changes in cation-chloride co-transporter expression: NKCC1), a cation-Cl^- importer, is highly expressed in neuronal precursor cells during early brain development[52,53], while the expression of the K^+-Cl^- cotransporter 2 (KCC2), a cation-Cl^- exporter, increases after the first postnatal week[10-12]. This increased KCC2 transporter expression might provide a central mechanism for the depolarization to hyperpolarization switch of GABAergic transmission via progressive reduction of $[Cl^-]_{in}$[13,50,54-57].

The $GABA_AR$ switch from depolarizing to hyperpolarizing occurs at P7 in the hippocampus, cortex, amygdala[12,44-49]. Our study suggests that this switch is delayed in the mPFC compared to primary somatosensory cortex and it takes place between P10 and P20. Specifically, we show that increased $GABA_AR$ activity leads to enhanced fEPSPs in neonatal mPFC (P10), suggesting that the $GABA_AR$ function is depolarizing in the mPFC at P10. This hypothesis is further supported by decreased levels of KCC2 transporter in the neonatal mPFC. Our results could have implications for understanding the delayed maturation of mPFC compared to other cortical areas, which may depend on a combination of a delayed switch from depolarizing-to-hyperpolarizing function of $GABA_AR$ and maturation of interneurons.

Interneurons and mPFC development

Recordings of $Lhx6^+$- interneurons indicate that both passive and active properties are regulated by age and reach values that better resemble adult MGE-derived interneurons. Specifically, we have found that the input resistance and AP width decrease while the AP rate

of rise increases in the mPFC at P20 compared to P10. In part, similar findings have been identified for PV^+ cells in the hippocampus[58,59] and SST^+ cells in the anterior cingulate cortex[39]. On the other hand, the AHP amplitude is still quite immature in the mPFC at P20, compared to PV^+, SST^+ interneurons in primary sensory areas or the hippocampus and compared to adult mPFC[39,40,58]. Therefore, it is likely that the physiological properties of PV+ and SST+ interneurons in the mPFC continue to change past the third postnatal week.

Our knowledge on the neonatal physiology of mPFC is very limited. It has been shown that PV expression is lowest in juveniles and increases during adolescence to levels similar to those observed in adulthood[60]. Furthermore, PV expression is not evident in the neonatal period and emerges during the pre-juvenile period in the mPFC[61-64]. Our results agree with these findings, as PV expression was detected during the pre-juvenile period in the mPFC. Dysfunction of PV^+ interneurons is sufficient to result in behavioural (and other) changes similar to those observed in a range of psychiatric disorders[65].

In addition, our study has identified decreased excitatory and increased inhibitory synaptic function between the second and third postnatal weeks. We show that the frequency of sIPSCs in layer II/III pyramidal cells of mPFC increases from neonatal to pre-juvenile period, consistent with the developmental trajectory of IPSCs in layer III pyramidal neurons of monkey PFC[66] and mouse mPFC[67].

Pyramidal neurons and network activity

It has been suggested that spontaneous network activity changes from local, highly synchronized to more diffuse from the second to the third postnatal weeks, in the primary sensory cortices[68,69]. Oscillatory activity in the mPFC first emerges at P15[70]. In this study, we have found increased spiking activity in the mPFC during the third, compared to the second postnatal week. This occurred despite the decreased excitatory and increased inhibitory synaptic function, but could be explained partly by the developmental increase of AP amplitude and rate of rise in the mPFC layer II/III pyramidal neurons, which could be due to the on-going maturation of sodium channels in pyramidal neurons.

Studies in developing mPFC pyramidal neurons have proposed that there is a unique sensitive time window for synaptic maturation of these neurons from individual cortical layers. During rat mPFC layer V development, the intrinsic properties, synaptic inputs and

morphology of pyramidal neurons develop together during early postnatal life. While the greatest changes were reported during the first ten days after birth, the adult-like properties emerged after the end of the third week (P21)[71]. This study confirms that the second postnatal week is a period of rapid growth, similar to that in other neocortical regions by combining functional and structural measurements of developing pyramidal neurons in mouse mPFC[72,73].

Developmental PFC malformation leads to cognitive disorders in adulthood

The neonatal functional maturation of GABAergic circuits and E/I (excitation to inhibition) balance are critical for PFC-dependent behaviours and plasticity in the adult while their malfunction leads to many psychiatric disorders[65,74,75]. From the prenatal period to late adolescence, the PFC network is highly vulnerable to genetic and environmental factors[76], since the mPFC is one of latest cortical regions to develop[77]. While many studies have focused on understanding several developmental processes during adolescence[78], our knowledge regarding the cellular and network developmental processes during the perinatal period is significantly limited, despite significant evidence showing that environmental manipulations during this period manifest as complex psychiatric and neurologic disorders in adulthood [79].

The delayed developmental shift of GABA action in various mouse models mimicking human brain disorders have been investigated, including the maternal immune activation model[80,81], the Scn1a and SCn1b mouse models of Dravet syndrome, the 22q11.2 deletion syndrome[82,83] and the Fmr1 deficient model of fragile X syndrome[84]. In the latter study, early postnatal correction of GABA depolarization (bumetanide-treated) led to sufficient normalization of the mature BC network[84]. The impaired KCC2 has been proposed as a potential therapeutic target of epilepsies by many studies in animal models and human patients[85].

Our study focuses in understanding the early developmental cellular and physiological mechanisms of mPFC circuits, before adolescence, and proposes that the neonatal mPFC compared to BC exhibits a delayed switch from depolarization to hyperpolarization function of $GABA_AR$. Our results raise the possibility that the delayed maturation of mPFC compared to other cortical areas depends on a combination of a delayed switch from depolarization to hyperpolarization function of the $GABA_AR$ and delayed maturation of interneurons.

Methods

All *in vitro* experiments with mice took place under an experimental protocol approved by the Research Ethics Committee and by our Institutional Animal Care and Use Committee that has been approved by the Veterinarian Authorities Office (protocol license no. 93164). Experiments were carried out by trained scientists and in accordance with the 3R principles. *In vivo* experiments were performed in compliance with the German laws and the guidelines of the European Community for the use of animals in research and were approved by the local ethical committee (015/17, 015/18).

Animals

The *in vitro* experiments were performed on male C57Bl/6J; Lhx6Tg(Cre); R26R-YFP+/+ mice from animal facility of IMBB-FORTH were used. For the *in vivo* experiments, timed-pregnant C57BL/6J mice from the animal facility of the University Medical Center Hamburg-Eppendorf were used. The day of vaginal plug detection was defined as embryonic day (E)0.5, whereas the day of birth was defined as P0. The offspring of both sexes are used for *in vivo* electrophysiology recordings. All procedures were performed according to the European Union ethical standards outlined in the Council Directive 2010/63EU of the European Parliament on the protection of animals used for scientific purposes.

Mice were housed with their mothers and provided with standard mouse chow and water ad libitum, under a 12 h light/dark cycle (light on at 7:00 am) with controlled temperature (21◦C). The P10 experimental group includes ages P9-P11 and the P20 group includes ages P19-P21, also referred to as second and third postnatal weeks or neonatal and pre-juvenile, respectively. All efforts were made to minimize both the suffering and the number of animals used.

In vitro extracellular recordings

Slice Preparation*:* Mice (P10 and P20) were decapitated under halothane anesthesia. The brain was removed promptly and placed in ice cold, oxygenated (95% O_2 –5% CO_2) artificial cerebrospinal fluid (aCSF) containing (in mM): 125 NaCl, 3.5 KCl, 26 $NaHCO_3$, 1 $MgCl_2$ and 10 glucose (pH = 7.4, 315 mOsm/l). The brain was blocked and glued onto the stage of a vibratome (Leica, VT1000S). Rostrocaudal coronal slices (400 µm thick) containing either the mPFC (prefrontal cortex) or the BC (barrel cortex) region were selected and transferred to a

545 submerged chamber, which was continuously superfused with oxygenated (95% O_2 –5% CO_2)
546 aCSF containing (in mM): 125 NaCl, 3.5 KCl, 26 $NaHCO_3$, 2 $CaCl_2$, 1 $MgCl_2$ and 10 glucose (pH
547 = 7.4, 315 mOsm/l) at room temperature (RT). The slices were allowed to equilibrate for at
548 least 1 h in this chamber before recordings began. Slices were then transferred to a
549 submerged recording chamber, continuously superfused with oxygenated (95% O_2 –5% CO_2)
550 aCSF (same constitution as the one used for maintenance of brain slices) at RT during
551 recordings.
552 Data Acquisition: Electrophysiological recordings were performed in all experimental groups
553 under the same conditions as described below. Pulled glass micropipettes were filled with
554 NaCl (2M) and placed in layers II/III of PFC and BC. Platinum/iridium metal microelectrodes
555 (Harvard apparatus United Kingdom, 161 Cambridge, United Kingdom) were placed on layer
556 II/III of the mPFC and the BC, about 300 µm away from the 1MΩ recording electrode, and
557 were used to evoke field excitatory postsynaptic potentials (fEPSPs). Local field potentials
558 (LFPs) were amplified using a headstage with selectable high pass filter of 30 Hz to remove
559 any offsets coupled to a Dagan BVC-700A amplifier, amplified 100 times and low-pass filtered
560 at 1-kHz. A notch filter was used to eliminate line frequency noise at 30 Hz. Signals were
561 digitized using the ITC-18 board (InstruTech, Inc.) on a PC with custom-made procedures in
562 IgorPro (Wavemetrics, Inc.) and stored on a PC hard drive. All voltage signals were collected
563 at a sampling frequency of 100 kHz (fs = 100 kHz).
564 For evoked fEPSPs, the electrical stimulus consisted of a single square waveform of
565 100 µs duration given at intensities of 0.1– 0.3 mA (current was increased from 0.1 mA to 0.3
566 mA, with 0.1 mA steps) generated by a stimulator equipped with a stimulus isolation unit
567 (World Precision Instruments, Inc.). The effect of $GABA_AR$ activation was investigated by bath
568 application of 2 µM Diazepam ($GABA_AR$ agonist). Diazepam was acquired from the Pharmacy
569 of the University General Hospital in Heraklion as a 5 mg/ml solution and was diluted in aCSF
570 during recordings.
571 Data Analysis: Data were analyzed using custom-written procedures in IgorPro software
572 (Wavemetrics, Inc.). No additional high-pass filters were applied to the raw data. For evoked
573 recordings, the peak values of the fEPSP were measured using the minimum value of the
574 synaptic response (4–5 ms following stimulation) and were compared to the baseline value
575 prior to stimulation. Both parameters were monitored in real- time in every experiment. A
576 stimulus–response curve was then plotted using stimulation intensities between 0.1 and 0.8

mA, in 0.1 mA steps. For each different intensity level, two traces were acquired and averaged.

***In vitro* patch-clamp recordings**

Slice Preparation: Mice were decapitated under halothane anesthesia. The brain was removed immediately and coronal slices of mPFC and BC (300–350 µm thick), using a vibratome (Leica, VT1000S, Leica Biosystems) were prepared from mice at the ages of P10 and P20 in ice-cold oxygenated (95% O_2 - 5% CO_2) modified choline-based aCSF (in mM) 0.5 $CaCl_2$, 7 mM $MgSO_4$; NaCl replaced by an equimolar concentration of choline). Slices were incubated for 30min at 32°C in an oxygenated normal aCSF containing (in mM): 126 NaCl, 3.5 KCl, 1.2 NaH_2PO_4, 26 $NaHCO_3$, 1.3 $MgCl_2$, 2.0 $CaCl_2$, and 10 D-glucose, pH 7.4, 315 mOsm/l. Slices were allowed to equilibrate for at least 30 min at RT before being transferred to the recording chamber. During recordings, slices were perfused at a rate of 4 ml/min with continuously aerated (95% O_2-5% CO_2) normal aCSF at RT.

Data Acquisition: Neurons were impaled with patch pipettes (5–7 MΩ) and recorded in the whole-cell configuration, either in the current-clamp or voltage-clamp mode. For current-clamp experiments, the composition of the intracellular solution was: 130 mM K-$MeSO_4$, 5 mM KCl, 5 mM NaCl, 10 mM HEPES, 2.5 mM Mg-ATP, and 0.3 mM GTP, 265–275 mOsm, pH 7.3. For voltage-clamp experiments, the composition of the intracellular solution was: 120 mM Cs-gluconate, 20mM CsCl, 0.1 mM $CaCl_2$, 1 mM EGTA, 0.4 mM Na-guanosine triphosphate, 2mM Mg-adenosine triphosphate, 10 mM HEPES. No correction from liquid junction potential was applied between the pipette and the aCSF. Whole-cell measurements were low-pass filtered at 5 kHz using an Axopatch 200B amplifier (Molecular Devices, Inc). Recordings were digitized with the ITC-18 board (Instrutech, Inc) on a PC using custom-made codes in IgorPro (Wavemetrics, Inc). All signals were collected at a sampling frequency of 20kHz.

Data Analysis: Data were analyzed using custom-written codes in IgorPro software (Wavemetrics, Inc.). For passive membrane properties, the resting membrane potential (RMP, mV) was measured within 3 min after establishing the whole-cell configuration, and monitored throughout the experiment. To measure input resistance, a 500ms step-pulse protocol was used with current stimulation from -200pA to +50pA. The input resistance (R_{in}, MΩ) was measured by plotting the steady-state voltage deflection in an I-V plot and

609 calculating the slope of the best fit line curve (R_{in}=V/I). The τ_m (membrane time constant, ms)
610 was obtained by fitting a single exponential curve to the voltage deflection at -50pA, and the
611 membrane capacitance (C_m) was calculated using the formula $C_m = \tau_m/R_{in}$. In addition, the
612 number of spikes generated in response to a 500ms step-pulse range from +100pA to +300pA
613 was measured.
614 To measure action potentials (APs) properties, we applied small supra-threshold 5ms
615 step-pulse currents to the cell from -65mV. The active properties were measured at the
616 minimum current stimulation (Rheobase, pA) that generated an AP. The AP threshold (mV)
617 was calculated by taking the first derivative of the voltage trace, defining a threshold and
618 identifying the voltage level at that time point. The rate of rise of the AP (dV/dt, mV/ms) was
619 the maximum value of that first derivative trace. The AP amplitude (mV) was defined as the
620 voltage difference between AP threshold and AP peak. The AP duration (ms) was calculated
621 by the full width of the waveform at the half maximal amplitude (half-width). The
622 afterhyperpolarization (AHP) minimum (mV) was defined as the minimum voltage right after
623 the AP. The AHP amplitude (mV) was calculated as the difference between the AHP minimum
624 and the AP threshold. The AHP time (ms) was defined as the time duration from the time
625 point of AP threshold to the AHP minimum.
626 The composition of our intracellular solution resulted in chloride reversal potential of
627 -60mV and Na^+/K^+ reversal potential of +10mV. This allowed for measurements of
628 spontaneous excitatory postsynaptic currents (sEPSCs) to be recorded at -60mV and of
629 spontaneous inhibitory postsynaptic currents (sIPSCs) to be recorded at +10mV.
630 Automatically selected events were subsequently visually monitored to discard erroneously
631 included noise. The events showing only single peaks were selected for kinetics analysis. All
632 currents detected from every single neuron were averaged. The peak amplitude was
633 calculated as the maximum current value. The time constant of the decay phase was detected
634 by curve fitting with a single exponential decay function.
635
636 ***In vivo* extracellular recordings**
637 Surgery: Multisite extracellular recordings were performed in the PFC of P8–P10 (n=13) and
638 P20–P23 (n=14) C57/BL mice with both sexes. Mice were under urethane anesthesia
639 (intraperitoneal injection, 1 mg/g body weight; Sigma-Aldrich) before surgery. The bone over
640 the mPFC (0.8 mm anterior to bregma, 0.1–0.5 mm right to the midline) was carefully

641 removed. One-shank electrodes with 4 recording sites (0.4–0.8 MΩ impedance, 100 µm
642 spacing, NeuroNexus) was inserted into PFC at a depth of 1.9 mm from the skull surface.
643 Electrodes were labelled with DiI (1,1′-dioctadecyl-3,3,3′,3′-tetramethyl indocarbocyanine;
644 Invitrogen) to confirm their position after histological assessment post-mortem. One silver
645 wire was inserted into the cerebellum to serve as ground and reference electrode.
646 Data Acquisition: A recovery period of 10 min following the insertion of electrodes before
647 acquisition of data was provided. Data acquired during the first 30 min of recording were used
648 for analysis to ensure similar state of anesthesia in all investigated pups. Extracellular signals
649 were bandpass filtered (0.1 Hz to 5 kHz) and digitized (32 kHz) with a multichannel
650 extracellular amplifier (Digital Lynx SX, Neuralynx) and the Cheetah acquisition software
651 (Neuralynx).
652 Data Analysis: Data were imported and analyzed off-line using custom-written tools in
653 MATLAB software version 7.7 (MathWorks). Multiple unit activity (MUA) is detected when
654 negative deflections exceeding five times the SD of the bandpass filtered (500–5000 Hz)
655 signals.
656
657 **Immunohistochemistry**
658 Mice at the age of P10 and P20 were perfused with 4% paraformaldehyde, followed by
659 fixation with the same solution for 1h at 4◦C, followed by cryoprotection and preparation of
660 12 µm cryostat sections as previously described[88]. Primary antibodies used were rat
661 monoclonal anti-GFP (Nacalai Tesque, Kyoto, Japan, 1:5000), rabbit polyclonal anti-GFP
662 (1:500; Minotech biotechnology, Heraklion, Greece) and rabbit polyclonal anti- parvalbumin
663 (PV) (Swant, Bellinzona, Switzerland; 1:2000. Secondary antibodies used were goat anti-rat-
664 Alexa Fluor-488, goat anti-rabbit Alexa Fluor-488, and goat anti-rabbit-Alexa Fluor-555
665 (Molecular Probes, Eugene, OR, United States, 1:800). Images were obtained with a confocal
666 microscope (Leica TCS SP2, Leica, Nussloch, Germany). For each age group (P10, P20), 2-4
667 10µm-thick sections from each mouse brain were selected, all including the mPFC and BC.
668
669 **RNA *In Situ* Hybridization**
670 Non-radioactive *in situ* hybridization experiments were performed on cryostat sections
671 (12µm thick, see immunochemistry) according to the protocol described[86]. Riboprobe was
672 prepared by *in vitro* transcription and was specific Somatostatin (SST)[37].

673

674 **Nissl Staining**

675 Cryostat sections (12µm thick, see immunochemistry) were incubated in 1:1 100%
676 ethanol:chloroform overnight at RT. Then, sections were rehydrated for 1 min in 100%, 95%
677 ethanol solutions and dH_2O at RT, followed by a 10-min incubation in 0.1% cresyl violet
678 solution at 50°C. Sections were then dehydrated with dH_2O, 95%, 100% ethanol and xylene
679 for 5 min and coverslipped with permount. Images from whole sections were obtained in 5×
680 magnification of a light microscope (Axioskop 2FS, Carl Zeiss AG, 268 Oberkochen, Germany)
681 and merged using Adobe Photoshop CC 2015, Adobe Systems, Inc.

682

683 **Analysis for Immunochemistry, *in situ* hybridization and Nissl staining**

684 The background color of each cropped image was converted to black, while the cells were
685 colored blue. The images were loaded into Matlab, where the number of 'blue' pixels was
686 counted per area (mm^2). Each cell was assumed to be composed of four pixels. Therefore, the
687 number of cells was measured as the total number of 'blue' pixels divided by four [87]. An
688 average number was calculated for the number of neurons from mPFC and BC sections from
689 each developmental group.

690

691 **Western blots**

692 Mice were decapitated following cervical dislocation, the brain was quickly removed, placed
693 in ice cold PBS (phosphate-buffered saline) and then positioned on a brain mould, where 1.5
694 mm slices were taken containing the mPFC and BC. The slices were placed on dry ice, and the
695 prelimbic area of mPFC was dissected out and stored at -80°C. The BC was also isolated from
696 the corresponding slices and stored at -80°C. Frozen tissue blocks were lysed in a solution
697 containing (in mM) HEPES 50, NaCl 150, MgCl2 1.5, EGTA 5, Glycerol 1%, Triton-X100 1%,
698 1:1000 protease inhibitors cocktail. Proteins ran on 8.5% bis-acrylamide gel and were
699 transferred onto a nitrocellulose membrane (Whatman GmbH, Dassel, Germany). The
700 membrane was blocked, incubated in rabbit polyclonal anti-K+/Cl-Cotransporter (KCC2)
701 (Merck KGaA, Darmstadt, Germany, 1:1000) or rabbit monoclonal anti-GAPDH (Cell Signaling
702 Technology Europe BV, Leiden, Netherlands, 1:1000), washed, incubated in secondary goat
703 anti-rabbit IgG Horseradish Peroxidase Conjugate antibody (Invitrogen, 1:5000), and digitally
704 exposed using the Molecular Imaging system ChemiDoc (BioRad Laboratories, Inc, California,

U.S.A.). Analysis of KCC2 and GAPDH expression was performed with ImageJ software, and the raw values of KCC2 from each sample were normalized to their respective GAPDH values.

Statistical analysis

Statistical analyses were performed in Microsoft Office Excel 2007 and GraphPad Prism Software 7.0. Data are presented as mean ± standard error of mean (SEM). Normality distribution and equality of variances of dataset were tested with the Kolmogorov-Smirnov test normality test. The null hypothesis was rejected for a >5%. When four experimental groups (P10 mPFC, P20 mPFC, P10 BC and P20 BC) were assessed and two variables were taken into consideration (age and brain area), data were analyzed with a two-way ANOVA with Fisher LSD, Sidak's or Tukey's multiple comparisons (electrophysiological recordings and cell counting). When three groups (P10 mPFC, P20 mPFC and P10 BC) data were analyzed with one- way ANOVA (electrophysiological recordings). For the comparison of *in vivo* spiking activity between P10 and P20, statistical analyses were performed with MATLAB. Significant differences were detected by one-way ANOVA. Significance levels of *$p < 0.05$, **$p < 0.01$, ***$p < 0.001$ or ****$p < 0.0001$ were tested. For comparison of Western blot analysis, the significant effect of each developmental age group from mPFC and BC was assessed using Student's t-test depending on the experiment.

Reference:

1. Khazipov, R. *et al.* Early motor activity drives spindle bursts in the developing somatosensory cortex. *Nature* **432,** 758–761 (2004).
2. Khazipov, R. & Luhmann, H. J. Early patterns of electrical activity in the developing cerebral cortex of humans and rodents. *Trends in Neurosciences* **29,** 414–418 (2006).
3. Allene, C. *et al.* Sequential Generation of Two Distinct Synapse-Driven Network Patterns in Developing Neocortex. *J. Neurosci.* **28,** 12851–12863 (2008).
4. Khazipov, R., Minlebaev, M. & Valeeva, G. Early gamma oscillations. *Neuroscience* **250,** 240–252 (2013).
5. Brockmann, M. D., Pöschel, B., Cichon, N. & Hanganu-Opatz, I. L. Coupled Oscillations Mediate Directed Interactions between Prefrontal Cortex and Hippocampus of the Neonatal Rat. *Neuron* **71,** 332–347 (2011).
6. Southwell, D. G. *et al.* Intrinsically determined cell death of developing cortical interneurons. *Nature* **491,** 109–113 (2012).
7. Ben-Ari, Y., Khalilov, I., Kahle, K. T. & Cherubini, E. The GABA Excitatory/Inhibitory Shift in Brain Maturation and Neurological Disorders. *The Neuroscientist* **18,** 467–486 (2012).

8. Kirmse, K. *et al.* GABA depolarizes immature neurons and inhibits network activity in the neonatal neocortex in vivo. *Nature Communications* **6,** 7750 (2015).
9. Mòdol, L. *et al.* Assemblies of Perisomatic GABAergic Neurons in the Developing Barrel Cortex. *Neuron* 1–18 (2019). doi:10.1016/j.neuron.2019.10.007
10. Ben-Ari, Y. Refuting the challenges of the developmental shift of polarity of GABA actions: GABA more exciting than ever! 1–18 (2012). doi:10.3389/fncel.2012.00035/abstract
11. Ben-Ari, Y. Developing networks play a similar melody. *Trends in Neurosciences* **24,** 353–360 (2001).
12. Ben-Ari, Y., Gaiarsa, J. L., Tyzio, R. & Khazipov, R. GABA: A Pioneer Transmitter That Excites Immature Neurons and Generates Primitive Oscillations. *Physiological Reviews* **87,** 1215–1284 (2007).
13. Ben-Ari, Y. Excitatory actions of gaba during development: the nature of the nurture. *Nat Rev Neurosci* **3,** 728–739 (2002).
14. Burgard, E. C. & Hablitz, J. J. Developmental changes in NMDA and non-NMDA receptor-mediated synaptic potentials in rat neocortex. *Journal of Neurophysiology* **69,** 230–240 (1993).
15. Kriegstein, A. R., Suppes, T. & Prince, D. A. Cellular and synaptic physiology and epileptogenesis of developing rat neocortical neurons in vitro. *Developmental Brain Research* **34,** 161–171 (1987).
16. McCormick, D. A. & Prince, D. A. Post-natal development of electrophysiological properties of rat cerebral cortical pyramidal neurones. *The Journal of Physiology* **393,** 743–762 (1987).
17. Bahrey, H. L. P. & Moody, W. J. Early Development of Voltage-Gated Ion Currents and Firing Properties in Neurons of the Mouse Cerebral Cortex. *Journal of Neurophysiology* **89,** 1761–1773 (2003).
18. Ramoa, A. S. & McCormick, D. A. Developmental changes in electrophysiological properties of LGNd neurons during reorganization of retinogeniculate connections. *J. Neurosci.* **14,** 2089–2097 (1994).
19. Bartolini, G., Ciceri, G. & Marin, O. Integration of GABAergic Interneurons into Cortical Cell Assemblies: Lessons from Embryos and Adults. **79,** 849–864 (2013).
20. Le Magueresse, C. & Monyer, H. GABAergic Interneurons Shape the Functional Maturation of the Cortex. *Neuron* **77,** 388–405 (2013).
21. Hensch, T. K. The Power of the Infant Brain. *Nature Publishing Group* **314,** 64–69 (2016).
22. Guo, Z. V. *et al.* Flow of Cortical Activity Underlying a Tactile Decision in Mice. *Neuron* **81,** 179–194 (2014).
23. Fuster, J. *The Prefrontal Cortex*. (Academic Press, 2015).
24. Van De Werd, H. J. J. M., Rajkowska, G., Evers, P. & Uylings, H. B. M. Cytoarchitectonic and chemoarchitectonic characterization of the prefrontal cortical areas in the mouse. *Brain Struct Funct* **214,** 339–353 (2010).
25. Heidbreder, C. A. & Groenewegen, H. J. The medial prefrontal cortex in the rat: evidence for a dorso-ventral distinction based upon functional and anatomical characteristics. *Neuroscience & Biobehavioral Reviews* **27,** 555–579 (2003).
26. Best, J. R. & Miller, P. H. A Developmental Perspective on Executive Function. *Child Development* **81,** 1641–1660 (2010).

27. Casey, B. J., Giedd, J. N. & Thomas, K. M. Structural and functional brain development and its relation to cognitive development. *Biological Psychology* **54,** 241–257 (2000).
28. Kolb, B. *et al.* Experience and the developing prefrontal cortex. *Proc. Natl. Acad. Sci. U.S.A.* **109,** 17186–17193 (2012).
29. Tsujimoto, S. The prefrontal cortex: functional neural development during early childhood. *The Neuroscientist* **14,** 345–358 (2008).
30. Kroeze, Y. *et al.* Transcriptome Analysis Identifies Multifaceted Regulatory Mechanisms Dictating a Genetic Switch from Neuronal Network Establishment to Maintenance During Postnatal Prefrontal Cortex Development. *Cerebral Cortex* 1–19 (2017). doi:10.1093/cercor/bhw407
31. Schubert, D., Martens, G. J. M. & Kolk, S. M. Molecular underpinnings of prefrontal cortex development in rodents provide insights into the etiology of neurodevelopmental disorders. **20,** 795–809 (2014).
32. Diamond, A. in *Principles of Frontal Lobe Function* 466–503 (Oxford University Press, 2005). doi:10.1093/acprof:oso/9780195134971.003.0029
33. Bitzenhofer, S. H., Sieben, K., Siebert, K. D., Spehr, M. & Hanganu-Opatz, I. L. Oscillatory Activity in Developing Prefrontal Networks Results from Theta-Gamma-Modulated Synaptic Inputs. *CellReports* **11,** 486–497 (2015).
34. Bitzenhofer, S. H. *et al.* Layer-specific optogenetic activation of pyramidal neurons causes beta-gamma entrainment of neonatal networks. *Nature Communications* **8,** 14563 (2017).
35. Clancy, B., Darlington, R. B., Neuroscience, B. F.2001. Translating developmental time across mammalian species. *Elsevier* **105,** 7–17 (2001).
36. DeFelipe, J. & Fariñas, I. The pyramidal neuron of the cerebral cortex: Morphological and chemical characteristics of the synaptic inputs. *Progress in Neurobiology* **39,** 563–607 (1992).
37. Liodis, P. *et al.* Lhx6 Activity Is Required for the Normal Migration and Specification of Cortical Interneuron Subtypes. *Journal of Neuroscience* **27,** 3078–3089 (2007).
38. Huguenard, J. R., Hamill, O. P. & Prince, D. A. Developmental changes in Na+ conductances in rat neocortical neurons: appearance of a slowly inactivating component. *Journal of Neurophysiology* **59,** 778–795 (1988).
39. Pan, G., Yang, J.-M., Hu, X.-Y. & Li, X.-M. Postnatal development of the electrophysiological properties of somatostatin interneurons in the anterior cingulate cortex of mice. *Nature Publishing Group* 1–12 (2017). doi:10.1038/srep28137
40. Yang, J. M., Zhang, J., Yu, Y. Q., Duan, S. & Li, X. M. Postnatal Development of 2 Microcircuits Involving Fast-Spiking Interneurons in the Mouse Prefrontal Cortex. *Cerebral Cortex* **24,** 98–109 (2013).
41. Forloni, G., Hohmann, C., Research, J. C. D. B.1990. Developmental expression of somatostatin in mouse brain. I. Immunocytochemical studies. *Elsevier* **53,** 6–25 (1990).
42. Bendotti, C., Hohmann, C., Forloni, G., Brain, R. R. D.1990. Developmental expression of somatostatin in mouse brain. II. In situ hybridization. *Elsevier* **53,** 26–39 (1990).

43. Del Rio, J. A., Soriano, E. & Ferrer, I. Development of GABA-immunoreactivity in the neocortex of the mouse. *J. Comp. Neurol.* **326,** 501–526 (1992).
44. Ben-Ari, Y., Cherubini, E., Corradetti, R. & Gaiarsa, J. L. Giant synaptic potentials in immature rat CA3 hippocampal neurones. *The Journal of Physiology* **416,** 303–325 (1989).
45. Gulledge, A. T. & Stuart, G. J. Excitatory Actions of GABA in the Cortex. *Neuron* **37,** 299–309 (2003).
46. LoTurco, J. J., Owens, D. F., Heath, M. J. S., Davis, M. B. E. & Kriegstein, A. R. GABA and glutamate depolarize cortical progenitor cells and inhibit DNA synthesis. *Neuron* **15,** 1287–1298 (1995).
47. Luhmann, H. J. & Prince, D. A. Postnatal maturation of the GABAergic system in rat neocortex. *Journal of Neurophysiology* **65,** 247–263 (1991).
48. Martina, M., Royer, S. & Paré, D. Cell-Type-Specific GABA Responses and Chloride Homeostasis in the Cortex and Amygdala. *Journal of Neurophysiology* **86,** 2887–2895 (2001).
49. Owens, D. F., Boyce, L. H., Davis, M. B. E. & Kriegstein, A. R. Excitatory GABA Responses in Embryonic and Neonatal Cortical Slices Demonstrated by Gramicidin Perforated-Patch Recordings and Calcium Imaging. *J. Neurosci.* **16,** 6414–6423 (1996).
50. Rivera, C. *et al.* The K+/Cl- co-transporter KCC2 renders GABA hyperpolarizing during neuronal maturation. *Nature* **397,** 251–255 (1999).
51. Kaila, K. & Voipio, J. Postsynaptic fall in intracellular p H induced by GABA-activated bicarbonate conductance. *Nature* **330,** 163–165 (1987).
52. Yamada, J. *et al.* Cl− uptake promoting depolarizing GABA actions in immature rat neocortical neurones is mediated by NKCC1. *The Journal of Physiology* **557,** 829–841 (2004).
53. Plotkin, M. D., Snyder, E. Y., Hebert, S. C. & Delpire, E. Expression of the Na-K-2Cl cotransporter is developmentally regulated in postnatal rat brains: A possible mechanism underlying GABA's excitatory role in immature brain. *J. Neurobiol.* **33,** 781–795 (1997).
54. Ganguly, K., Schinder, A. F., Wong, S. T. & Poo, M.-M. GABA Itself Promotes the Developmental Switch of Neuronal GABAergic Responses from Excitation to Inhibition. *Cell* **105,** 521–532 (2001).
55. Fiumelli, H., Cancedda, L. & Poo, M.-M. Modulation of GABAergic Transmission by Activity via Postsynaptic Ca2+-Dependent Regulation of KCC2 Function. *Neuron* **48,** 773–786 (2005).
56. Lu, J., Karadsheh, M. & Delpire, E. Developmental regulation of the neuronal-specific isoform of K-CL cotransporter KCC2 in postnatal rat brains. *J. Neurobiol.* **39,** 558–568 (1999).
57. Dzhala, V. I. *et al.* NKCC1 transporter facilitates seizures in the developing brain. *Nature Medicine 2005 11:11* **11,** 1205–1213 (2005).
58. Doischer, D. *et al.* Postnatal Differentiation of Basket Cells from Slow to Fast Signaling Devices. *J. Neurosci.* **28,** 12956–12968 (2008).
59. Miyamae, T., Chen, K., Lewis, D. A. & González-Burgos, G. Distinct physiological maturation of parvalbumin-positive neuron subtypes in mouse prefrontal cortex. *J. Neurosci.* 3325–16–48 (2017). doi:10.1523/JNEUROSCI.3325-16.2017

60. Caballero, A., Flores-Barrera, E., Cass, D. K. & Tseng, K. Y. Differential regulation of parvalbumin and calretinin interneurons in the prefrontal cortex during adolescence. *Brain Struct Funct* **219,** 395–406 (2014).
61. Spampanato, J. & Sullivan, R. Development and physiology of GABAergic feedback excitation in parvalbumin expressing interneurons of the mouse basolateral amygdala. *Physiological …* **4,** e12664–15 (2016).
62. del Rio, J., De Lecea, L., Ferrer, I. & Soriano, E. The development of parvalbumin-immunoreactivity in the neocortex of the mouse. **81,** 247–259 (1994).
63. de Lecea, L., del Ri o, J. A. & Soriano, E. Developmental expression of parvalbumin mRNA in the cerebral cortex and hippocampus of the rat. *Molecular Brain Research* **32,** 1–13 (1995).
64. Zheng, K., An, J. J., Yang, F. & Xu, W. TrkB signaling in parvalbumin-positive interneurons is critical for gamma-band network synchronization in hippocampus. in (2011). doi:10.1073/pnas.1114241108/-/DCSupplemental
65. Ferguson, B. R. & Gao, W.-J. PV Interneurons: Critical Regulators of E/I Balance for Prefrontal Cortex-Dependent Behavior and Psychiatric Disorders. *Front Neural Circuits* **12,** 479–13 (2018).
66. González-Burgos, G. *et al.* Functional Maturation of GABA Synapses During Postnatal Development of the Monkey Dorsolateral Prefrontal Cortex. *Cerebral Cortex* **25,** 4076–4093 (2015).
67. Kroon, T., van Hugte, E., van Linge, L., Mansvelder, H. D. & Meredith, R. M. Early postnatal development of pyramidal neurons across layers of the mouse medial prefrontal cortex. *Scientific Reports* **9,** 5037–16 (2019).
68. Golshani, P. *et al.* Internally Mediated Developmental Desynchronization of Neocortical Network Activity. *J. Neurosci.* **29,** 10890–10899 (2009).
69. Frye, C. G. & MacLean, J. N. Spontaneous activations follow a common developmental course across primary sensory areas in mouse neocortex. *Journal of Neurophysiology* **116,** 431–437 (2016).
70. Bitzenhofer, S. H., Poepplau, J. A., Chini, M., Marquardt, A. & Hanganu-Opatz, I. Activity-dependent maturation of prefrontal gamma oscillations sculpts cognitive performance. *bioRxiv* 1–39 (2019). doi:10.1101/558957
71. Zhang, Z., Jiao, Y.-Y. & Sun, Q.-Q. Developmental maturation of excitation and inhibition balance in principal neurons across four layers of somatosensory cortex. *Neuroscience* **174,** 10–25 (2011).
72. Zhu, J. J. Maturation of layer 5 neocortical pyramidal neurons: amplifying salient layer 1 and layer 4 inputs by Ca2+ action potentials in adult rat tuft dendrites. *The Journal of Physiology* **526,** 571–587 (2000).
73. Romand, S., Wang, Y., Toledo-Rodriguez, M. & Markram, H. Morphological Development of Thick-Tufted Layer V Pyramidal Cells in the Rat Somatosensory Cortex. *Front. Neuroanat.* **5,** (2011).
74. Kilb, W. Development of the GABAergic System from Birth to Adolescence. *The Neuroscientist* **18,** 613–630 (2012).
75. Benes, F. M. Deficits in Small Interneurons in Prefrontal and Cingulate Cortices of Schizophrenic and Schizoaffective Patients. *Archives of General Psychiatry* **48,** 996–1001 (1991).
76. Andersen, S. L. Trajectories of brain development: point of vulnerability or window of opportunity? *Neuroscience & Biobehavioral Reviews* **27,** 3–18 (2003).

928 77. Huttenlocher, P. R. Morphometric study of human cerebral cortex development.
929 *Neuropsychologia* **28,** 517–527 (1990).
930 78. Caballero, A., Granberg, R. & Tseng, K. Y. Mechanisms contributing to prefrontal
931 cortex maturation during adolescence. *Neuroscience & Biobehavioral Reviews* 1–
932 29 (2016). doi:10.1016/j.neubiorev.2016.05.013
933 79. Weinberger, D. R. Physiologic Dysfunction of Dorsolateral Prefrontal Cortex in
934 Schizophrenia. *Archives of General Psychiatry* **43,** 114 (1986).
935 80. Fernandez, A. *et al.* The GABA Developmental Shift Is Abolished by Maternal
936 Immune Activation Already at Birth. *Cerebral Cortex* **130,** e1447–11 (2018).
937 81. Corradini, I. *et al.* Maternal Immune Activation Delays Excitatory-to-Inhibitory
938 Gamma-Aminobutyric Acid Switch in Offspring. *Biological Psychiatry* **83,** 680–691
939 (2018).
940 82. Yuan, Y. *et al.* Delayed maturation of GABAergic signaling in the Scn1a and Scn1b
941 mouse models of Dravet Syndrome. *Scientific Reports* 1–16 (2019).
942 doi:10.1038/s41598-019-42191-0
943 83. Amin, H., Marinaro, F., De Pietri Tonelli, D. & Berdondini, L. Developmental
944 excitatory-to-inhibitory GABA-polarity switch is disrupted in 22q11.2 deletion
945 syndrome: a potential target for clinical therapeutics. *Scientific Reports* 1–18
946 (2017). doi:10.1038/s41598-017-15793-9
947 84. He, Q. *et al.* Critical period inhibition of NKCC1 rectifies synapse plasticity in the
948 somatosensory cortex and restores adult tactile response maps in fragile X mice.
949 *Mol Psychiatry* **8,** 109–16 (2018).
950 85. Moore, Y. E., Kelley, M. R., Brandon, N. J., Deeb, T. Z. & Moss, S. J. Seizing Control
951 of KCC2: A New Therapeutic Target for Epilepsy. *Trends in Neurosciences* **40,** 555–
952 571 (2017).
953 86. Schaeren-Wiemers, N. & Gerfin-Moser, A. A single protocol to detect transcripts
954 of various types and expression levels in neural tissue and cultured cells: in situ
955 hybridization using digoxigenin-labelled cRNA probes. *Histochemistry* **100,** 431–
956 440 (1993).
957 87. Konstantoudaki, X., Chalkiadaki, K., Tivodar, S., Karagogeos, D. & Sidiropoulou, K.
958 Impaired synaptic plasticity in the prefrontal cortex of mice with developmentally
959 decreased number of interneurons. *Neuroscience* 1–13 (2016).
960 doi:10.1016/j.neuroscience.2016.02.048
961 88. Vidaki, M., Tivodar, S., Doulgeraki, K., Tybulewicz, V., Kessaris, N., Pachnis, V.,
962 Karagogeos, D. (2012). Rac1-Dependent Cell Cycle Exit of MGE Precursors and
963 GABAergic Interneuron Migration to the Cortex Cerebral Cortex 22(), 680 - 692.
964
965

966 **Acknowledgements:**

967 Authors are grateful to Dr. Myrto Denaxa for her comments on the manuscript, to
968 Emmanuella Foinikianaki for her help with Matlab analysis and histology and to Giasemi
969 Eptaminitaki for her help in *in situ* hybridization experiments. They also would like to thank all
970 the members of Karagogeos and Sidiropoulou Labs and the animal facility of the IMBB for

help with experiments. This study was co-financed through the Operational Program "Education and Lifelong Learning" of the National Strategic Reference Framework – Research Funding Program (EDBM34) by a grant to DK (10040) and through the BIOIMAGING-GR, National Roadmap for Research Infrastructures from the European Union (European Social Fund-ESF) and Greek National Funds. KK has been a recipient of the Manasaki fellowship and a Medical School fellowship of the University of Crete and a poster award at the 27th Hellenic Society for Neuroscience Meeting.

Author Contributions:

All experiments were conceived and designed by K.K., K.S., and D.K. All experiments performed by K.K. Data were analyzed by K.K., K.S. and discussed with D.K., X.X. and I.L.H.-O. X.X. carried out and analyzed the *in vivo* experiments. Manuscript was written by K.K., D.K. and K.S. All authors discussed and commented on the manuscript.

998 **Table 1. Intrinsic electrophysiological properties of pyramidal neurons and interneurons in**
999 **mPFC and BC at P10 and P20.**

Pyramidal Neurons				
	P10 mPFC	P20 mPFC	P10 BC	P20 BC
Resting membrane potential, RMP (mv)	-65.55 ± 0.70, n=9	-65.63 ± 0.47, n=10	-65.14 ± 0.84, n=9	-65.45 ± 0.82, n=8
Input Resistance (MΩ)	202.4 ± 9.12, n=9	179.8 ± 17.35, n=10	182.3 ± 21.74, n=7	145.6 ± 13.9, n=7
Membrane time constant, τm (ms)	16.49 ± 1.97, n=7	18.8 ± 2.16, n=10	17.64 ± 2.13, n=7	20.42 ± 1.5, n=6
Membrane Capacitance, Cm (pF)	**70.64 ± 10.12, n=7**	111 ± 7.79, n=9	**80.24 ± 7.69, n=7**	145.9 ± 17.59, n=5
AP amplitude (mv)	**89.6 ± 1.82, n=8**	104.5 ± 3.13, n=12	**83.27 ± 5.12, n=8**	102.9 ± 5.35, n=7
Rate of rise of AP: dV/dt (mv/ms)	**146.5 ± 12.98, n=8**	232.6 ± 12.38, n=11	151.8 ± 19.28, n=7	204.6 ± 28.84, n=8
Duration of AP: Half-width (ms)	1.779 ± 0.07779, n=8	1.76 ± 0.08, n=14	1.94 ± 0.19, n=7	1.77 ± 0.14, n=8
Rheobase (pA)	266.7 ± 23.57, n=9	217.9 ± 15.38, n=14	227.8 ± 26.5, n=9	237.5 ± 33.74, n=8
Threshold (mv)	-64.89 ± 0.89, n=9	-65.96 ± 1.09, n=13	-63.43 ± 1.52, n=7	-65,65 ± 0.7, n=6

1000

Interneurons			
	P10 mPFC	P20 mPFC	P10 BC
Resting membrane potential, RMP (mv)	-64.81 ± 2.11, n=6	-62.22 ± 0.94, n=8	-63.29 ± 1.54, n=9
Input Resistance (MΩ)	**391.7 ± 73.62, n=8**	129.2 ± 23.91, n=8	159.8 ± 17.89, n=9
Membrane time constant, τm (ms)	**36.94 ± 8.18, n=8**	20.72 ± 8.37, n=6	10.29 ± 2.45, n=8
Membrane Capacitance, Cm (pF)	**80.9 ± 10.09, n=6**	272.6 ± 109.8, n=6	49.2 ± 3.67, n=7
AP amplitude (mv)	**78.92 ± 4.15, n=6**	76.41 ± 8, n=8	57.56 ± 3.84, n=8
Rate of rise of AP: dV/dt (mv/ms)	90.49 ± 3.7, n=6	166.7 ± 21.48, n=6	**66.41 ± 4.24, n=8**
Duration of AP: Half-width (ms)	2.24 ± 0.17, n=6	**1.31 ± 0.15, n=8**	2.49 ± 0.23, n=7
Rheobase (pA)	170 ± 20, n=5	150 ± 15.43, n=7	162.5 ± 15.67, n=8
Threshold (mv)	-61.52 ± 1.5, n=5	-56.58 ± 2.94, n=8	-54.79 ± 3, n=9
AHP amplitude (mv)	-4.65 ± 0.95, n=4	-5.96 ± 0.72, n=6	**-13.99 ± 1.69, n=7**
AHP time (ms)	14.64 ± 1.29, n=5	13.26 ± 3.07, n=7	16.57 ± 2.47, n=7

1001 ± represents the standard error of mean and n represents the number of cells. **Bold** numbers indicate significant
1002 differences after post-hoc analysis (more details in figure legends).
1003

1004

1005

1006